Stable numeric scheme for diffusion equation with a stiff transport

G. V. Pereverzev [a] G. Corrigan [b]

[a] *IPP-EURATOM Fusion Association, Max-Planck-Institut für Plasmaphysik, D-85748, Garching, Germany*

[b] *EURATOM/UKAEA Fusion Association, Culham Science Centre, Abingdon, Oxon, OX14 3DB, UK*

Abstract

It is known that the anomalous transport in fusion devices is governed by gradient-driven instabilities and is characterised by an offset linear dependence of the heat and particle fluxes on the corresponding gradients. The dependence is very strong so that a small change in gradients causes a huge variation of fluxes thus giving rise to the so called stiff transport. This feature makes the standard numeric schemes for a parabolic equation strongly unstable so that plasma simulations with transport codes require very small time steps. In this paper, a modification of the standard finite difference scheme is suggested that eliminates this kind of numerical instability. It is shown that the implementation of the technique allows the time step for stiff transport models to be increased by several orders of magnitude. Generalisation to more advanced numeric schemes and to a system of parabolic equations is straightforward.

Key words: fusion, tokamak, stiff transport, numeric stability
PACS: 52.55.Fa, 52.25.Fi, 02.60.Lj

1 Introduction

Plasma confinement in fusion devices has been extensively studied for about four decades, and the first numerical models were created at the end of sixties. From the very beginning it was understood that the particle and energy losses observed in fusion devices were strongly underestimated by the classic

Email address: pereverzev@ipp.mpg.de (G. V. Pereverzev).

transport theories based on the Coulomb collisions [1,2]. The enhanced non-classic transport was attributed to a plasma turbulence and referred to as the anomalous transport. The plasma turbulence is quite a complex and versatile phenomenon [3] therefore various models and approaches have been tested, but a consensus regarding the anomalous transport mechanism is not yet fully established. Nevertheless, it is widely recognised that the particle and energy transport in tokamaks is mainly determined by the gradient-driven drift-type instabilities and many efforts are now invested in studies of this type of transport.

Consistent computer simulation of the turbulent transport requires complicated nonlinear codes that are based on a gyro-fluid or more sophisticated plasma description in a real geometry. These codes are very time consuming, so their results can be used either for direct comparison with experiment in a quite limited space and time region or as a basis for building much more simplified models that can be used on a wide parameter, time and space domain. In the recent years, massive and correlated efforts were applied to construct reduced transport models for tokamak plasmas [4-7].The common feature of these models is that they are all based essentially on a first-principle description and, unlike early transport models, do not rely on any heuristic considerations. However, the complicated background physics of these theory-based models is substantially simplified in different ways, and different methods of construction are employed. As a result, the physical effects taken into account in different models are not exactly the same and, in addition, even similar effects are sometimes treated differently.

For this reason one cannot concentrate on a single model. All, or most of them, have to be studied in parallel and verified against the available experimental data in order to find weak point of each model, identify missing physics and then to construct a more complete and reliable model with higher predictable capabilities. It is also accepted that the ITER project [8], presently based on the phenomenological and empirical scaling laws, should be re-evaluated on the basis of the theory-based models.

A computer tool for conducting this programme is called a tokamak transport code. The code describes plasma behaviour in a tokamak device whose magnetic structure is described by a set of enclosed torii. Most of these torii are fully covered by a single magnetic field line and therefore they are called magnetic surfaces. Because the equilibration along the magnetic field lines is extremely fast, the plasma characteristics within each toroidal magnetic surface are assumed to be homogeneous. Across these surfaces the plasma density, temperature and other relevant plasma parameters obey diffusion equations. The particle and energy fluxes are related to their gradients by the matrix which is provided by the first-principle transport models as described above. Therefore the core of a transport code is a set of 1D parabolic equations.

The set of equations is very simple and usually causes no problem. However, when the theory-based transport models are employed, then a relevant simulation can become extremely time consuming. This is because the standard numeric schemes applied to these transport models result in highly unstable algorithms thus imposing severe limitations on the time step of integration. The cause of this numerical problem is usually attributed to the physics of the turbulence driven transport. The anomalous energy (or particle) flux associated with a given type of instability is zero when the instability is not excited but it switches on and rapidly increases beyond the instability threshold. The strong dependence of the diffusion coefficient on the driving gradient is responsible for the numerical instability. The transport models are called stiff models by analogy with stiff ODE that are characterised by greatly different eigenvalues and also require very small time steps unless special numerical techniques are applied.

In addition, one has to take into account that many plasma problems of interest include different time scales and require very long runs, far beyond the time required for the relaxation of fast anomalous transport processes. Moreover, the wide variety of tokamak regimes and uncertainty of numerous additional parameters adds to the complexity of the transport modelling. This requires multiple runs for essentially the same physical cases in order to estimate a sensitivity of the results to a number of insufficiently well known plasma characteristics. All of these circumstances make the usage of the theory-based models impractical unless a drastic improvement of the usual numerical schemes is developed and implemented in the code. This paper proposes such a modification of the standard numerical scheme for a parabolic equation that allows the time step to be increased by orders of magnitude.

In Section 2 we formulate the problem and introduce a simple model equation that reproduces all of the main properties of the stiff transport model. In the next section, qualitative arguments are presented that should clarify a reason of the numerical instability. Then a possible way of improvement is discussed and a modification of the standard finite difference algorithm is proposed. Numerical examples of the usage of the new algorithm are presented in Section 4. The discussions, possible extensions and conclusions are given in Section 5.

2 Formulation of the problem

2.1 Differential equation and difference scheme

Consider a simplified diffusion equation for the function $u = u(x,t)$ of the space x and the time t coordinates

$$u_t = (Du_x - Vu)_x + S, \qquad 0 < x < 1, \qquad t > 0. \tag{1}$$

The subscripts t and x denote partial derivatives with respect to time and space, u is a generic plasma parameter as density, temperature, etc., D and V are the diffusion coefficient and the convective velocity, respectively, that depend on x, u and u_x, $S = S(u,x)$ is a source term. The combination $q = Vu - Du_x$ in the brackets of Eq. (1) will be referred to as a flux of the quantity u. We assume that appropriate boundary and initial conditions are provided. It is also understood that u and S can be vectors, D and V matrices but this is immaterial for our consideration.

Without going in details we can write the numeric scheme for Eq. (1) in the standard form

$$\begin{aligned} &\frac{\hat{u}_i - u_i}{\tau} + \frac{q_{i+1/2} - q_{i-1/2}}{h} = S_i, \qquad i = 0, 1, \ldots, N \\ &q_{i+1/2} = -D_{i+1/2}\frac{\alpha_{i+1/2}\hat{u}_{i+1} - \beta_{i+1/2}\hat{u}_i}{h}, \end{aligned} \tag{2}$$

where τ and h are the time and space steps respectively. The integer subscript i is related to the grid cell centre x_i and the half-integer $i + 1/2$ to the cell boundary $\bar{x}_{i+1/2} = (x_{i+1} + x_i)/2$. The hat denotes quantities evaluated at the next time step $t + \tau$. All other quantities are evaluated at the time t. The approximation for the flux in Eq. (2) can be done in many different ways. In this paper we use the exponential scheme proposed in [9] that gives very good results for any reasonable values of D and V. In this scheme

$$\begin{aligned} &\alpha(\xi) = \frac{\xi}{1 - e^{-\xi}}, \qquad \xi = -\frac{hV}{D} \\ &\alpha_{i+1/2} = \alpha(\xi_{i+1/2}), \qquad \beta_{i+1/2} = \alpha_{i+1/2} - \xi_{i+1/2}, \end{aligned} \tag{3}$$

where ξ is called the grid Peclet number. For example, the finite difference scheme (2)–(3) is exact for the steady state solution of Eq. (2) in regions where D and V are constant and $S = 0$, for any value of the Peclet number [9]. In general, the scheme has the aproximation order $\mathcal{O}(h^2)$ in space and

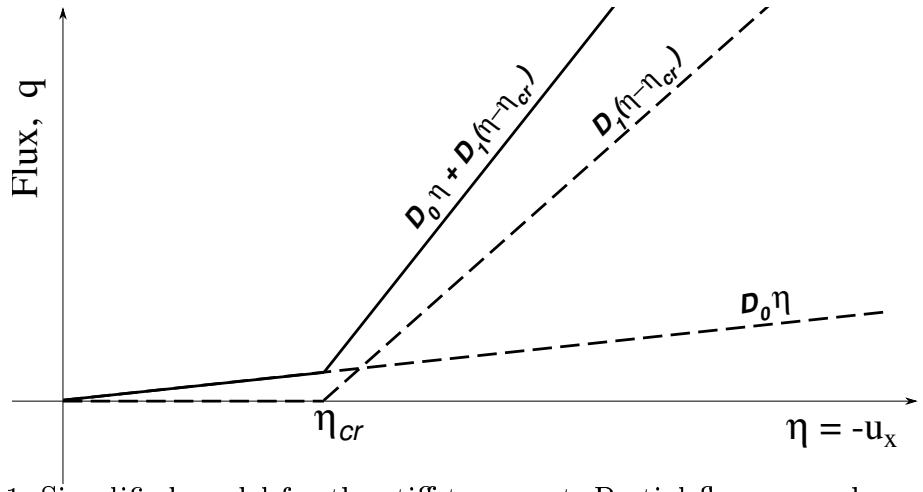

Fig. 1. Simplified model for the stiff transport. Partial fluxes are shown with dashed lines, total flux with a solid line.

$\mathcal{O}(\tau)$ in time. The finite difference scheme also preserves the number of particles (energy) and thus complies with the conservation law. The only property discussed below is the numerical stability that really has a crucial impact on the usage of the theory-based transport models. All other numerical properties that are very important in other contexts are not addressed here.

2.2 Model equation

As discussed in the introduction, the functions D, V, and S result from solving complicated sets of equations that are essentially independent from Eq. (1). Although it is not always correct physically, most of the theory-based transport models return $V = 0$. This happens because the models calculate the entire fluxes as the combination $q = Vu - Du_x$. Separating this flux into the partial components and, consequently, a separate calculation of D and V is possible but requires additional computations. Moreover, often it is not clear if this splitting is appropriate and really justified. Therefore it is usual to deal with the effective diffusivity $D_{an} = -q/u_x$ that under some circumstances can be also negative.

It follows that the typical dependence of the flux q on the plasma parameters has the form

$$q = -\left[D_0(x,u) + D_{an}(x,u,u_x)\right] u_x \tag{4}$$

where D_0 is the classic (or so called neo-classic) collisional diffusion and D_{an} includes contributions from different anomalous processes. For simplicity we

consider here only one such an anomalous process and start with the discussion of the simplest model

$$D_{an} = \begin{cases} D_1 \left(\eta - \eta_{cr}\right)/\eta, & \text{if} \quad \eta > \eta_{cr} > 0, \\ 0, & \text{if} \quad \eta < \eta_{cr}, \end{cases} \tag{5}$$

where $\eta = -u_x$. The dependence (5) is illustrated by Fig. 1. The classical flux is proportional to the gradient while the anomalous flux switches on when the gradient exceeds the threshold. Once $\eta > \eta_{cr}$ the flux rapidly increases because of $D_1 \gg D_0$. This strong inequality dominates all properties of the considered problem. It gives rise to the name stiff transport and is a cause of the numerical instability studied below. Typically, the diffusion D_0 is quite low so that, in practice, the gradient η increases until it reaches the threshold η_{cr}. Above η_{cr} a small enhancement of η drives a huge increase of the flux q and prevents further growth of the gradient. As a result, the whole plasma is beyond the threshold η_{cr} although the actual gradient η is always close to the value η_{cr}. As an exception, narrow space zones can exist that are called transport barriers. These zones with a large variations in the slope η could require a special treatment.

3 Numerical algorithm

3.1 Instability of the standard finite difference scheme

In practice, the dependence shown in Fig. 1 is not known. Neither η_{cr} nor D_1 can be easily derived. Instead, in every space point x one knows the parameter set $\{u, u_x\}$ and can calculate the classical flux $q_0 = -D_0 u_x$ and the anomalous flux q_{an} or, equivalently, $D_{an} = -q_{an}/u_x$. Consequently, the diffusion equation is simply

$$u_t = (D^{eff} u_x)_x + S \tag{6}$$

where $D^{eff} = D_0 + D_{an}$ is a known space function. The simplest difference representation of Eqs. (6) along the line of Eq. (2) is

$$\frac{\hat{u}_i - u_i}{\tau} = D^{eff}_{i+1/2} \frac{\hat{u}_{i+1} - \hat{u}_i}{h^2} - D^{eff}_{i-1/2} \frac{\hat{u}_i - \hat{u}_{i-1}}{h^2} + S_i, \quad i = 0, 1, \ldots, N. \tag{7}$$

We repeat that the accuracy of this numeric scheme with respect to the time step is rather low and can be substantially improved. However, it is not the

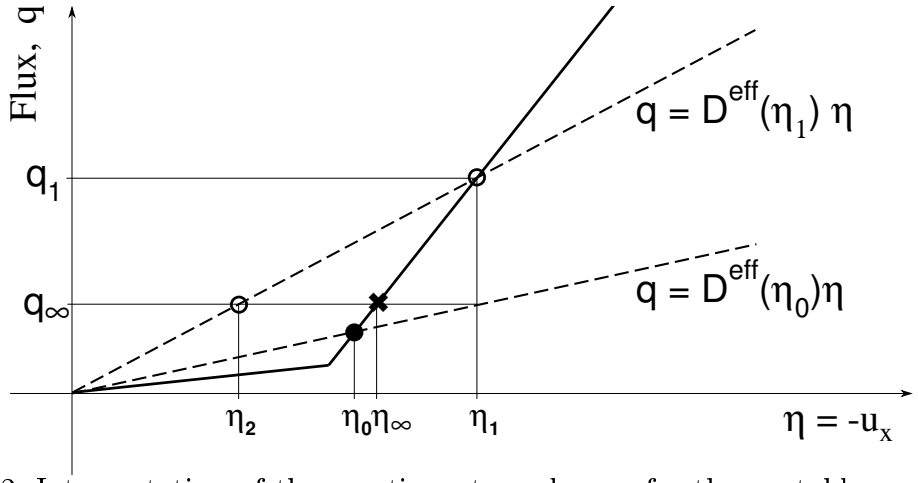

Fig. 2. Interpretation of the one-time-step advance for the unstable numerical scheme (7). Successive time steps are given by η_0, η_1, η_2, etc. The filled circle shows the current work point, cross shows the steady state solution. The solid line is the same as in Fig. 1.

subject of the current paper because all features of difference schemes discussed below are not directly related to the accuracy.

Consider now the properties of the solution given by Eq. (7) in more detail. Assume that a current work point is given by η_0 as shown with a filled circle in Fig. 2. Assume also that the steady state flux for these conditions can be achieved at η_∞ and is $q_\infty = D^{eff}\eta_\infty$ (cross in Fig. 2). The numerical scheme Eq. (7) implies that the flux is a linear function of u_x, $q = D^{eff}(\eta_0)\eta$. The function is shown in Fig. 2 by the dashed line crossing the filled circle. If the time step τ in Eq. (7) is large enough then the scheme will predict the gradient η_1 such that $q_\infty \approx D^{eff}(\eta_0)\eta_1$. Then the calculated flux $q_1 = D^{eff}(\eta_1)\eta_1$ (empty circle in Fig. 2) will exceed the expected flux q_∞ by a factor $D^{eff}(\eta_1)/D^{eff}(\eta_0) \gg 1$. It is easy to see that the subsequent time step will give $\eta_2 < \eta_0$ thus indicating a numerical instability that arises when the time step τ exceeds a certain threshold. By reducing the time step this instability would be suppressed, however, in real situation, this condition limits the time step to an extremely low value that is approximately a factor of 10^{-5} smaller than all physically relevant characteristic times of the problem. Under such a constraint any realistic modelling becomes very time consuming.

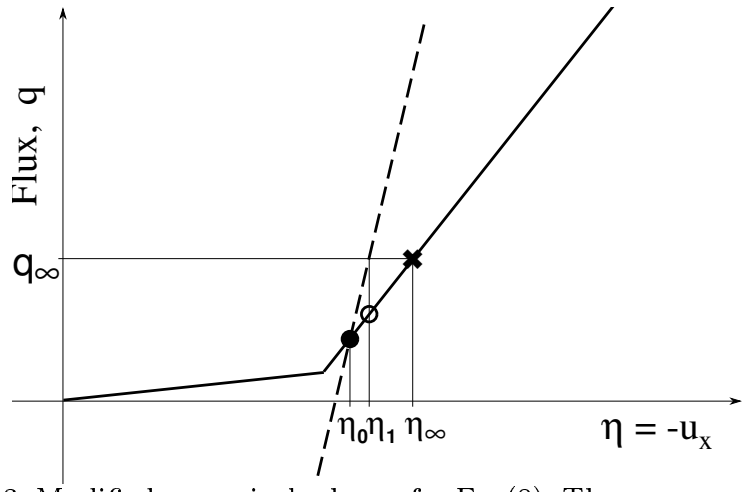

Fig. 3. Modified numerical scheme for Eq. (8). The sequence of time steps $\eta_0, \eta_1, \ldots$ is monotonic. The dashed line shows the modified flux in Eq. (8). The solid line is the same as in Fig. 1.

3.2 Stable finite difference scheme

The discussion of Fig. 2 suggests a direct way to overcome this difficulty. First of all consider a modification of Eq. (6)

$$u_t = (D^{eff} u_x + \bar{D} u_x - \bar{V} u)_x + S, \qquad \bar{V} = \bar{D} \frac{u_x}{u}. \tag{8}$$

The new equation (8) is identical to Eq. (6) at arbitrary $\bar{D}$ because the sum of added terms is identically zero. If the explicit numerical scheme is applied to Eq. (8) then again it will be equivalent to Eq. (6). However, the difference implementation for Eq. (8) along the line of (2)-(3) is not identical to that for Eq. (6). Indeed, for Eq. (8) we obtain the scheme (2) when D is replaced with $D^{eff} + \bar{D}$ and ξ with

$$\xi = -\frac{h\bar{V}}{D^{eff} + \bar{D}}. \tag{9}$$

The difference arises because the quantities u and u_x in brackets of Eq. (8) are calculated at $t + \tau$ while all other terms including $\bar{V}$ and ξ at t. Numerical properties of the new difference scheme are illustrated by Fig. 3. The dashed line here shows the dependence of the flux $q = q(u_x)$ in Eq. (8) at fixed D^{eff}, $\bar{D}$ and $\bar{V}$. Provided the value of $\bar{D}$ is high enough the slope of the dashed line $\bar{D}$ in the point η_0 is higher than that of the solid line $\partial q / \partial \eta$, i.e. $\bar{D} > D_0 + D_{an} = D^{eff}$.

The same qualitative consideration as before indicates that the time step started with η_0 ends up with $\eta = \eta_1$ that is in between η_0 and η_∞. For the simple model (5), the scheme (2), (9) is numerically stable. In more realistic cases, this kind of analysis is not possible. Moreover, the actual behaviour can be rather different. Nevertheless, the test runs described in the next section show very robust behaviour at large $\bar{D}$. Above some limit the quantity $\bar{D}$ can be anything while the quantity $\bar{V}$ has to be adjusted at each grid point in line with Eq. (8). In what follows we use $\bar{D} = \text{Const}$ although varying this quantity can provide further improvements.

It is obvious that the different numerical stability of the same difference scheme (2) as applied to the differentially equivalent equations (6) and (8) means that a non-vanishing term is added in the latter case. The term can be easily found analytically however its numeric computation is rather problematic since this would require calculation of the flux first in the old and then in the new scheme. Because the former can be made with very small time steps only, all advantage will be lost. However, such a computation is important because it gives a quantitative evaluation of the quality of the solution. In order to allow such an evaluation we do essentially the same transform in the difference (7) rather than in the differential (6) equation. The flux $q_{i+1/2} = D^{eff}_{i+1/2} \left(\hat{u}_i - \hat{u}_{i+1} \right) / h$ in Eq. (7) will be modified as

$$\begin{aligned} & q_{i+1/2} \quad \longrightarrow \quad q_{i+1/2} + \bar{q}_{i+1/2}, \\ & \bar{q}_{i+1/2} = -\frac{1}{h} \bar{D}_{i+1/2} \left[\alpha(\bar{\xi}_{i+1/2}) \hat{u}_{i+1} - \beta(\bar{\xi}_{i+1/2}) \hat{u}_i \right], \quad \bar{\xi}_{i+1/2} = \ln \frac{u_i}{u_{i+1}}. \end{aligned} \tag{10}$$

Using Eq. (3) one has

$$\bar{q}_{i+1/2} = -\frac{1}{h} \bar{D}_{i+1/2} \ln \frac{u_i}{u_{i+1}} \frac{u_i \hat{u}_{i+1} - u_{i+1} \hat{u}_i}{u_i - u_{i+1}}. \tag{11}$$

So far the quantity $\bar{D}$ has been considered as arbitrary therefore one can save computing time by replacing $\bar{D}$ with a very close quantity $\tilde{D}$

$$\tilde{D}_{i+1/2} = \bar{D}_{i+1/2} \frac{u_{i+1/2}}{u_i - u_{i+1}} \ln \frac{u_i}{u_{i+1}} = \bar{D}_{i+1/2} \left(1 + \mathcal{O}(h^2) \right). \tag{12}$$

It is seen that the difference between $\bar{D}$ and $\tilde{D}$ is of higher order in h than the accuracy of flux approximation in Eq. (10). Therefore in what follows we will not distinguish between the two quantities. Now the additional term (11) takes the form

$$\bar{q}_{i+1/2} = -\bar{D}_{i+1/2} \frac{u_i \hat{u}_{i+1} - u_{i+1} \hat{u}_i}{h \, u_{i+1/2}} = \mathcal{O}(\tau) + \mathcal{O}(h^2). \tag{13}$$

The quantity $\bar{q}_{i+1/2}$ is the difference approximation (2) of the zero flux $\bar{D}u_x - \bar{V}u$ included in Eq. (8). Unlike its differential prototype $q = \bar{D}\left[u\left(u_x/u\right) - u_x\right] \equiv 0$ the finite difference flux $\bar{q}_{i+1/2}$ is nonzero but, as shown in the next section, it can be easily computed at each time step.

3.3 Alternative view and interpretation

It is clear from our qualitative description that the main stabilisation effect is achieved due to the large additional term in the diffusive flux. In order to keep the total flux unchanged we added a compensating convective term. For the numerical stability it is significant that the newly added diffusive term is approximated implicitly. One can exploit the same idea in a different and probably more transparent form.

Instead of compensating for the additional implicit diffusive flux with an opposing convective flux, we can just subtract an explicit diffusive flux. The essential characteristics of the compensating term are the same in both schemes, namely an explicit dependence on u_x consistent with the offset linear dependence depicted in Fig. 3, and a full cancellation in steady state. In this alternative form, because there is no convective term, the exponential scheme is replaced with a central difference discretisation. Consequently, this approach results in an additional flux that can be expressed as

$$\tilde{q}_{i+1/2} = -\bar{D}_{i+1/2}\left(\frac{\hat{u}_{i+1} - \hat{u}_i}{h} - \frac{u_{i+1} - u_i}{h}\right) \tag{14}$$

at each grid point. A stabilising effect of the scheme Eq. (14) is comparable to that of Eq. (13).

First of all, we apply the Taylor expansion to the expressions (13), (14) and find

$$\bar{q} = -\tau\tilde{D}u\left(\ln u\right)_{xt} + \mathcal{O}(h^2) + \mathcal{O}(\tau^2) \tag{15}$$

and

$$\tilde{q} = -\tau\tilde{D}u_{xt} + \mathcal{O}(h^2) + \mathcal{O}(\tau^2), \tag{16}$$

respectively. It is seen that the added terms act as a mixed space-time derivative. Its stabilizing mechanism can be explained in a simple way. Following from our qualitative discussion in relation to Fig. 2, the considered numerical instability manifests itself as local oscillations in the gradient u_x. Moreover,

in the adjacent grid cells, these oscillations occur in the counter phase. Therefore, the small term (15) or (16) effectively suppresses the short-scale numerical instability. The relations (13) and (15) show that the artificially introduced fluxes $\bar{q}$ and $\tilde{q}$ go to zero as $\tau \to 0$ and when the solution $u(x,t)$ approaches the steady state. After the initial phase of fast relaxation one can increase the time step τ still keeping the error small. As mentioned this is essential when a problem includes different characteristic times which are much larger than that for the quantity u.

Second, it is seen that the error terms have a form of the flux of the quantity u. Any of them can be represented as the source term

$$\bar{S}_i = \frac{1}{h}\left(\bar{q}_{i+1/2} - \bar{q}_{i-1/2}\right) = \mathcal{O}(\tau), \qquad 1 < i < N. \tag{17}$$

This difference source does not contribute significantly to the global source $\int S dx$. Moreover, in the usual case of the boundary conditions $q_{1/2} = 0$ and $u_N = \text{Const}$ the global source

$$h\sum_{i=1}^{N} \bar{S}_i = \bar{q}_{N+1/2} - \bar{q}_{1/2} \tag{18}$$

vanishes. The local error (17) (or a similar one obtained by replacing $\bar{q}$ with $\tilde{q}$) introduced by the numerical scheme modification (10) should be compared with the local source S_i. If it is found that the error is too high then the time step has to be reduced. The final remark is that if needed the numerical scheme can be modified by subtracting the term (17) from the right hand side of Eq. (8) and employing iterations within each time step.

To conclude this section, we note that newly introduced terms do not change the order of approximation of the original scheme (2), (3) that formally remains $\mathcal{O}(\tau)+\mathcal{O}(h^2)$. This means that asymptotic properties of convergence to the exact solution for small τ and h remain unchanged so that the standard techniques for accuracy control remain applicable. On the other hand, one should be aware that local (in space) characteristics of the numerical scheme accuracy can be noticeably spoiled and that a continuous control of the additional error terms like Eqs. (15), (16) or Eq. (18) is indispensable.

4 Numeric examples

In this section we apply the proposed algorithm to a real tokamak simulation. As an example we consider the reference ITER inductive scenario [8].

The computations have been performed with the transport code ASTRA [10]. In order to highlight the numerical properties of the solution we reduce the full problem to a set of three coupled equations for the electron and ion temperatures and for the poloidal magnetic field. The plasma density profile is prescribed and kept fixed. Energy transport coefficients are calculated on the basis of the GLF23 transport model [6] that is currently considered as one of the most advanced model of this kind. On the other hand, this model is one of the most stiff and difficult for the numerical treatment. Therefore, if the algorithm is capable of handling GLF23 it should cope with all other models. Leaving aside the physics results of the simulation, we concentrate exclusively on its numeric aspects. All results presented below were obtained with the difference scheme modification described in Section 3.2. The alternative scheme Eq. (14) gives very similar results.

4.1 Time step control

In order to quantify the numerical stability of the algorithm we adopt the following control procedure for the time step τ. First we evaluate the quantity

$$\Delta_D = \max_i \left| \frac{\hat{D}_{an} - D_{an}}{D_{an}} \right| \leq \Delta_{tol} \tag{19}$$

that is considered as a measure of the numerical instability. The maximum in Eq. (19) is taken over all space grid nodes. If the quantity Δ_D exceeds a maximum allowed value of Δ_{tol} then the time step is repeated with a decreased τ. Otherwise, τ is increased and simulation continues. The algorithm maintains the approximate equality $\Delta_D(\tau) \approx \Delta_{tol}$. If Δ_{tol} is not very large the algorithm (19) always pushes the time step τ to the threshold of the numerical instability and defines a maximum tolerable time step τ_{tol} for a simulation with the given value of Δ_{tol}. As Δ_{tol} is increased, the resulting increase in time step gives rise to a numerical instability which manifests itself as a saw-like perturbation. This first emerges locally and then propagates over the grid with the velocity h/τ. In the simulations presented below Δ_{tol} was always small enough to keep the numerical instability at the marginal level. In this case, although a small perturbation with the amplitude Δ_{tol} is present it is localised at one or two places on the grid but does not expand.

The quantity D_{an} was selected as a sensor of the instability in line with the discussion in the previous section. A similar result can be obtained if in Eq. (19) D_{an} is replaced with the temperature gradient ∇u, i.e. with u_x in the notations of Section 3. It is worth noting that the quantity $u(x,t)$ does not show noticeable changes unless the numerical instability becomes uncontrollable. For this reason, selecting a working point slightly beyond the threshold of the

numerical instability is a reasonable choice for plasma applications.

4.2 Steady state phase

First we consider a steady state phase of a tokamak discharge. The code is started with arbitrary initial conditions and then runs until a steady state with respect to the plasma temperatures is achieved.[1] Since the constraint (19) is applied, the time step $\tau_{tol}(\Delta_{tol})$ is adjsuted automatically, and its value determined by the evolution of multiple plasma parameters in the selected tokamak scenario. In order to isolate the numerical characteristics of interest we consider the normalised quantity $\bar{\tau} = \tau_{tol}/\tau_{D0}$ where τ_{D0} is the time step forced by Eq. (19) at $\bar{D} = 0$. This quantity is plotted as a function of $\bar{D}$ in Fig. 4. As expected, $\bar{\tau}$ increases with $\bar{D}$. Moreover, above a certain threshold, $\bar{D} > \bar{D}_\infty$, the condition Eq. (19) does not restrict the time step any more so that a curve in Fig. 4 approaches a vertical asymptote. It means that the particular instability discussed here becomes stabilised and does not show up any more. Above this value of $\bar{D}$ the algorithm (19) does not limit the time step that grows until another control algorithm comes into play. However, this next limitation is usually related to numerical accuracy rather than to numerical stability.

Quantitatively, the behaviour discussed depends on many particular details of the simulation, but here we consider only the sensitivity of the algorithm to the parameter Δ_{tol}. If Δ_{tol} decreases then the limitation on $\bar{\tau}$ becomes more strict and the total curve scales down as shown in Fig. 4 with the dashed line. The "no-instability" threshold D_∞ increases, however, the qualitative behaviour does not change.

As seen from Fig. 4 a value of $\bar{D} \geq 50$ m^2/s is required in order to suppress the numerical instability if the latter is understood in the sense of Eq. (19) with a quite weak restriction for the relative variation. A stronger restriction requires an even higher value of $\bar{D}$. These quantities are much larger than the effective diffusion in this simulation, which is no more than $D^{eff} = 1$ m^2/s, indicating that D_∞ has no relation to D^{eff}. Our qualitative consideration in Section 3.2 shows that a more appropriate characteristic for $\bar{D}$ is the slope of the solid curve in Fig. 3 that is given by the derivative $q_\eta = \partial q/\partial\eta$. It was suggested that $\bar{D} > q_\eta$ was required for the numerical stability. In our example, q_η is a discontinuous function shown in Fig. 5. It is seen that $q_{\eta,i}$ varies between 20 m^2/s and 100 m^2/s that roughly explains the order of $\bar{D}$ required to enforce stability in accordance with the qualitative discussions

[1] With respect to the poloidal magnetic field there is no steady state but almost nothing changes in this time because the characteristic field diffusion time is more than by two orders of magnitude larger.

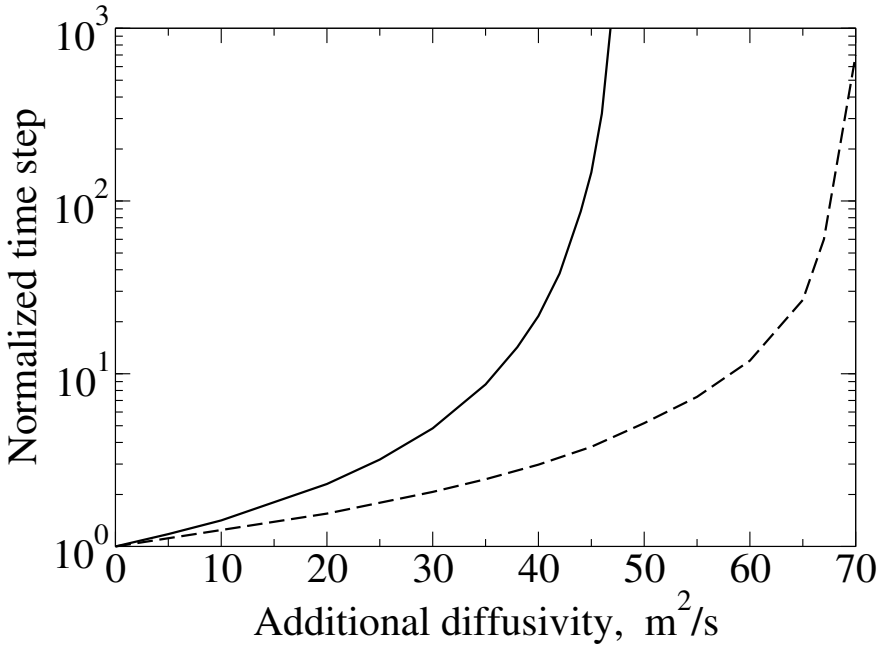

Fig. 4. Normalised time step $\bar{\tau}$ versus additional diffusion coefficient $\bar{D}$. The quantity $\bar{\tau}$ is plotted for two values of Δ_{tol}, 10% (solid line) and 5% (dashed line).

in Section 3. If $\bar{D} > q_\eta$ is fulfilled everywhere in space then the instability is not present. With decreasing $\bar{D}$ at a fixed time step, the instability first arises locally in the regions where $\bar{D} < q_\eta$, then the regions extend and the computation breaks down. As discussed the algorithm Eq. (19) keeps the time step just above the instability threshold.

It is worth noting that the condition $\bar{D} \geq q_\eta$ is quite limited and gives rather a rough estimate for a reasonable value of $\bar{D}$. This is because the variation of the flux q at each time step depends not only on the gradient η, but also on many other plasma parameters as in example shown with the dashed line in Fig. 5. In addition, changing the grid spacing can influence $\bar{D}$. Moreover, during the time evolution the spikes in Fig. 5 can move in space which drastically changes the local stability properties. All of these additional complications make it difficult to provide general recommendations for a suitable value of $\bar{D}$, and some investigation is required in differing applications.

4.3 Transient phase

In order to characterise the proposed numerical scheme in somewhat different circumstances we also consider the starting phase of the same tokamak simulation. This is a phase of the fast relaxation from artificial initial conditions to a steady state distribution. Again the time step limiting algorithm

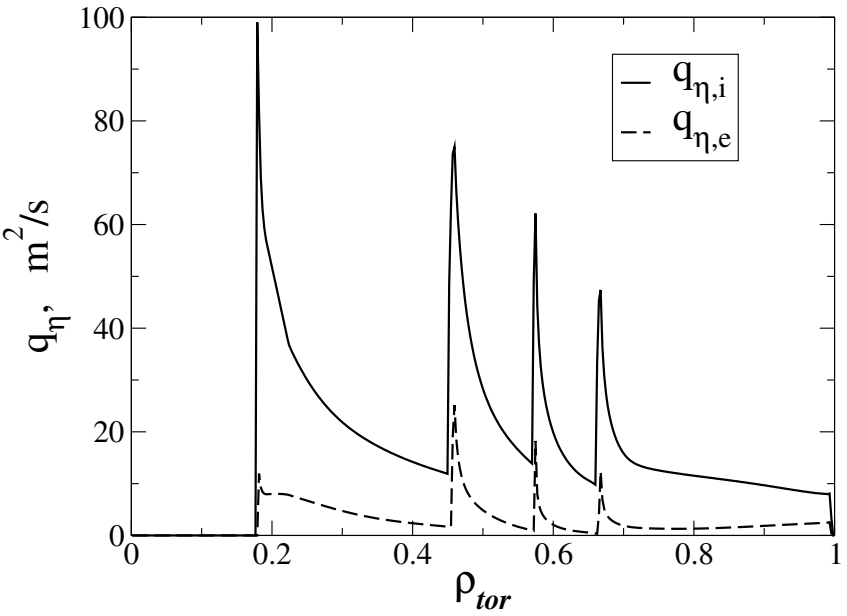

Fig. 5. Derivatives of the ion heat flux q_i with respect to the ion and electron temperature gradients are shown as functions of the plasma radius. Solid line shows $q_{\eta,i} = -\partial q_i/\partial(\nabla T_i)$, dashed line $q_{\eta,e} = -\partial q_i/\partial(\nabla T_e)$.

Eq. (19) was applied. The computer time required to reach the steady state is plotted in Fig. 6. As before, instead of the absolute magnitude we consider the quantity normalised to its value at $\bar{D} = 0$. In this case it is also possible to achieve an essential increase in the speed of the calculations. However, the gain in speed is not as large as for the steady state. This is because, during this initial phase of the fast relaxation, the numerical instability is only one of many reasons for time step limitation. Simultaneous variation of different plasma parameters imposes additional restrictions on the time step.

There can be many reasons for violation the inequality Eq. (19) that have nothing to do with the numerical stability of the difference scheme. The diversity of physics processes in a tokamak and the related complexity of in the transport codes result in many interdependencies in the code that also require controlling. Therefore, it is well to bear in mind that it does not make much sense to reduce Δ_{tol} below 5%. This observation is mainly valid for evolution of the discharge but is applicable also to its quasi-stationary phase. This usually requires additional control variables to limit the time step of the simulation.

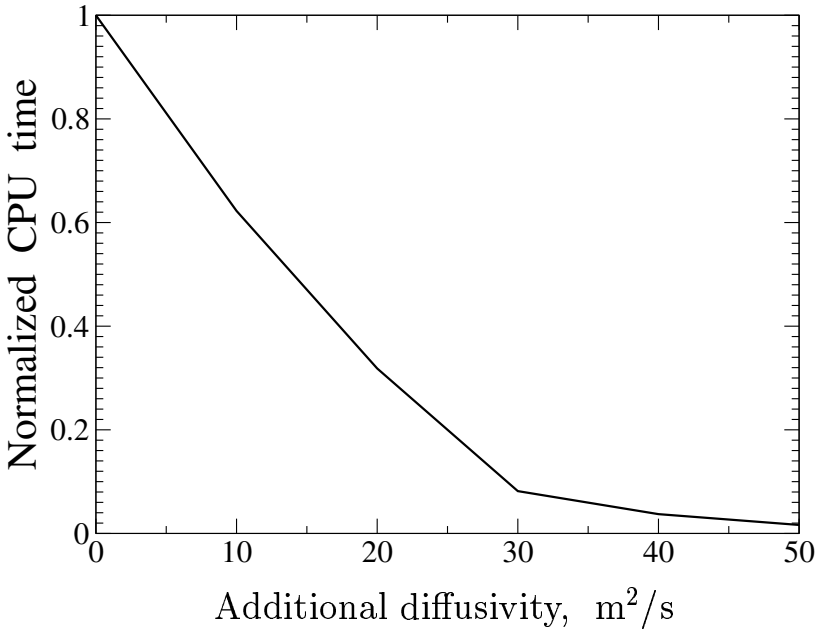

Fig. 6. Computer time needed to achieve a steady state as a function of the additional diffusivity at $\Delta_{tol} = 10\%$.

5 Summary and discussions

As discussed the paper addresses a specific case of finite difference schemes for a quasi-linear parabolic equation with a stiff transport. If applied to the energy transport, the stiffness means that the heat conductivity depends not only on the temperature but also has a strong dependence on the temperature gradient. In general, the tokamak plasma being a complex system shows a strongly non-linear offset response to any external influence such as energy, momentum and particle sources, etc. The discontinuity of the flux derivative with respect to the gradient causes a violent numerical instability of the standard finite difference scheme, both implicit and explicit.

A way of overcoming the difficulty is proposed that is based on including an additional large implicit diffusion flux in the equation and simultaneous subtracting the same flux in the form of convection or an explicit diffusion flux. Differentially the two terms are equivalent and the sum of those is exactly zero. However, the finite difference approximation introduces a non-zero correction in the numeric scheme that makes the algorithm stable. The correction can be thought of as a mixed space-time derivative with a small factor in front of it. A numerical error introduced by this additional term can easily be evaluated and used for monitoring the accuracy of the scheme.

As regards accuracy, for the standard numerical schemes, as Eqs. (2), (3), the time-step limit enforced by the stability requirement is extremely severe, and is typically many orders of magnitude more restrictive than that imposed by the accuracy condition. The gap is so large that even increasing the time step by a factor of 10^3 still does not bring the accuracy problem to the fore. In a few special cases only, it really becomes an issue. One of those is the transport barrier zone and its time evolution. Preliminary simulations show that the two different approaches discussed in Section 3.3 affect the barrier in opposite ways. Apparently a combination of both may be required to treat this problem in the most accurate and efficient way [11]. In any case, the scheme properties in this situation deserve a further detailed study. In other cases, the algorithm (19) gives quite reasonable control of the time step both from the point of stability and accuracy requirements.

Although the introduced error Eq. (13) (or Eq. (14)) increases with τ and $\bar{D}$ it usually remains unimportant as long as no developed instability is observed. This is because the error source is strongly localised in space and has a short-space-scale dipole nature. Therefore its integral is very close to zero not only over the whole grid but also over any space domain that covers several grid cells. As a result the total influence on the energy balance is negligible. Moreover, in many applications the details of the time evolution are not required, and for the steady state solution the introduced error vanishes everywhere. In addition, the sources and fluxes in transport modelling are often known only to an accuracy of 10% or worse. If, nevertheless, the correction (17) is found to be comparable with the physics source then, in order to avoid distortions of the time evolution, the term $\bar{D}$ and/or the time step τ have to be reduced during this phase of simulation. After approaching the steady state both can be increased again.

Conceptually, a similar technique was proposed in [12]. It was suggested to split the total anomalous flux in two pieces in line with

$$\begin{aligned} q(u,\eta) &= q(\eta_0) + \frac{\partial q(\eta_0)}{\partial \eta}(\eta - \eta_0) = V^{an}u + D^{an}\eta, \\ D^{an} &= \frac{\partial q(\eta_0)}{\partial \eta}, \qquad V^{an} = \frac{q(\eta_0) - D^{an}\eta_0}{u}. \end{aligned} \tag{20}$$

The distinction with our approach is that the quantity $\bar{D}$ introduced in Eq. (8) is not directly linked to $\partial q/\partial \eta$.

However, this formal difference has far reaching consequences. The quantity $\partial q/\partial \eta$ is shown in Fig. 5. As one can see it has a quite peculiar space dependence. Using the discontinuous function D^{an} as the diffusion coefficient can be challenging in itself. Moreover, the derivative $\partial q/\partial \eta$ does not encompass all dependencies of the flux. Although the dependence $q(u_x)$ is usually the

strongest one, q also depends on many other plasma parameters, and so the Taylor expansion in Eq. (20) is incomplete. Under certain circumstances variation of any of those can cause fast local change of D^{an} in space and time and this will have a stronger influence on the numerical stability stronger than u_x. Vicinities of the discontinuities in Fig. 5 are very sensitive in this respect. If a discontinuity moves over the grid then the time step of integration will be strongly reduced. In addition, Eq. (20) requires derivation of the numerically defined flux q that is usually the most expensive part of the simulation. With increasing complexity of the transport models the problem will become more and more limiting.

Most of these problems do not arise if the diffusion coefficient is a prescribed space function $\bar{D}$ that is taken independently of $\partial q/\partial \eta$. Nevertheless, one still has to bear in mind that a monitoring of quality should be applied to the solution. It means that the quantity $\bar{S}_i$ given by Eq. (17) is to be computed and compared with other sources and sinks in the equation. If it becomes large then either $\bar{D}$ or τ has to be reduced or a correction should be added to the right hand side. An additional remark can be made as regards the finite difference scheme. The compound flux in Eq. (8) consists of two large opposed fluxes, convective and diffusive. In terms of finite difference scheme the relative strength of the two fluxes is characterised by the Peclet number $\bar{P} = h\bar{V}/\bar{D} = h/L_u$ where $L_u = u/u_x$ is the characteristic length of variation of the parameter u. The estimate shows that $\bar{P}$ is usually rather small because the discretisation is always done in the way that the grid size h is much smaller than the characteristic size L_u. It means that the requirements for the numeric scheme are not very demanding.

In summary, a new numerical algorithm has been suggested for the stiff transport models. It exploits splitting the net flux in mutually compensating diffusive and convective components. The splitting includes a free parameter that is used to suppress the numeric instability of the standard difference scheme and allows the time step to be increased by several orders of magnitude. Differential interpretation of the algorithm shows that a new term is added. The term has a small factor and includes a mixed time-space derivative of the unknown quantity. This derivative effectively suppresses possible numerical instability. In this paper two versions of the approach are described for the simplest possible finite difference scheme for a parabolic equation. Generalisation to more advanced numeric schemes, non-equidistant grids, system of parabolic equations is straightforward.

Acknowledgement

This work was partly supported by the Engineering and Physical Sciences Research Council and by the European Communities under the Contract of Association between EURATOM and UKAEA. The views and opinions ex-

pressed here do not necessarily reflect those of the European Commission.

References

[1] S. I. Braginskii, in Reviews of Plasma Physics ed. by M. A. Leontovich, Vol. 1, (Consultants Bureau, New York, 1965) p. 205

[2] A. A. Galeev, R. Z. Sagdeev, in Reviews of Plasma Physics ed. by M. A. Leontovich, Vol. 7, (Consultants Bureau, New York 1979) p. 257

[3] B. B. Kadomtsev, O. P. Pogutse, in Reviews of Plasma Physics ed. by M. A. Leontovich, Vol. 5, (Consultants Bureau, New York, 1970) p. 249

[4] M. Kotschenreuther and W. Dorland, M. A. Beer and G.W. Hammet, Phys Plasmas **2** (1995) 2381

[5] J. Weiland, Collective Modes in Inhomogeneous Plasmas (IOP Publ., Bristol) 2000

[6] R. E. Waltz, G. M.Staebler, W. Dorland et al., Phys Plasmas **4** (1997) 2482

[7] G. Bateman, A. H. Kritz, J .E. Kinsey, A. J. Redd and J. Weiland, Phys Plasmas **5** (1998) 1793

[8] B. J. Green for the ITER International Team and Participant Team, Plasma Phys. Control. Fusion **45** (2003) 687

[9] S. V. Patankar, Numerical Heat Transfer and Fluid Flow (Hemisphere Publ. Corp., Washington, 1980)

[10] G. V. Pereverzev, P. N. Yushmanov, ASTRA - Automated System for Transport Analysis, Report IPP 5/98, Max-Planck-Institut für Plasmaphysik, Garching, 2002.

[11] G.V. Pereverzev, 35th EPS Conference on Plasma Physics, (Hersonissos, Greece, June, 2008) Contributed Paper P5.032.

[12] J. E. Kinsey, G. M. Staebler and R. E. Waltz, Phys. Plasmas, **9** (2002) 1678